Universiteit Antwerpen

This item is the archived peer-reviewed author-version of:

Positive and negative streamer propagation in volume dielectric barrier discharges with planar and porous electrodes

Reference:
Zhang Quan-Zhi, Zhang Li, Yang De-Zheng, Schulze Julian, Wang You-Nian, Bogaerts Annemie.- Positive and negative streamer propagation in volume dielectric barrier discharges with planar and porous electrodes
Plasma processes and polymers - ISSN 1612-8850 - Weinheim, Wiley-v c h verlag gmbh, 18:4(2021), e2000234
Full text (Publisher's DOI): https://doi.org/10.1002/PPAP.202000234
To cite this reference: https://hdl.handle.net/10067/1765650151162165141

uantwerpen.be
Institutional repository IRUA

Positive and negative streamer propagation in volume dielectric barrier discharges with planar and porous electrodes

Quan-Zhi Zhang[1,2], Li Zhang[2,3], De-Zheng Yang[3], Julian Schulze[1,4], You-Nian Wang[1] and Annemie Bogaerts[2]

[1]School of Physics, Dalian University of Technology, Dalian 116024, P.R. China

[2]Research Group PLASMANT, University of Antwerp, Universiteitsplein 1, B-2610 Antwerp-Wilrijk, Belgium

[3]Key Lab of Materials Modification, Dalian University of Technology, Dalian 116024, P.R. China

[4]Department of Electrical Engineering, Ruhr-University Bochum, Germany

Email: zhangli2013@mail.dlut.edu.cn, ynwang@dlut.edu.cn

Abstract

The spatio-temporal dynamics of volume and surface positive and negative streamers in a pin-to-plate volume dielectric barrier discharge is investigated. The discharge characteristics are found to be completely different for positive and negative streamers. First, the spatial propagation of a positive streamer is found to rely on electron avalanches caused by photoelectrons in front of the streamer head, whereas this is not the case for negative streamers. Second, our simulations reveal an interesting phenomenon of floating positive surface discharges, that develop when a positive streamer reaches a dielectric wall and which explains the experimentally observed branching characteristics. Third, we report for the first time the interactions between a positive streamer and dielectric pores, in which both the pore diameter and depth affect the evolution of a positive streamer.

Keywords: floating surface discharge, positive streamer, PIC/MCC simulation, pin-to-plate DBD

1. Introduction

Atmospheric pressure non-thermal dielectric barrier discharges (DBD) are widely used for various environmental applications, such as air pollution control, hydrocarbon reforming, greenhouse gas conversion, and nitrogen fixation [1–7]. Such plasmas typically consist of filamentary streamers. Understanding the fundamental physics of their generation and propagation is the basis for knowledge-based optimization of these societally highly relevant applications. A large part of the applied power is dissipated into a small volume, i.e. the streamer channels. The electrons inside these channels are very energetic and are able to induce complex chemical reactions, while the neutral gas remains at room temperature. Depending on the direction of the streamer propagation relative to the electric field inside one of these channels, there are two types of streamers, i.e. positive (same direction) and negative streamers (opposite direction). Negative streamers propagate in the direction of the electron drift in the local field, while positive streamers move against the drift direction and, therefore, require a source of electrons in front of the streamer head [8]. In most papers, the electron source in positive streamers is assumed to be photo-ionization. For instance, for DBDs operated in air, photo-ionization can be provided by excited nitrogen molecules emitting UV photons, which can ionize an oxygen molecule elsewhere in the discharge [9–12].

One of the differences between positive and negative streamers is their branching nature. For instance, in DBDs operated in air, the branching characteristics of positive streamers determine the streamer propagation direction and the area over which the discharge spreads [8,9,13]. This can be very important for plasma processing. Many efforts have, thus, been devoted to the investigation of positive streamer discharges, both experimentally and theoretically. Several models have been developed to investigate the underlying mechanisms and characteristics during positive streamer propagation in N_2-O_2 mixtures, including particle, fluid and hybrid models [14–19]. All of these models emphasize that the evolution of positive streamer discharges mainly depends on the presence of non-local photo-ionization around the streamer head in N_2-O_2 mixtures. Furthermore, the streamer branching profile largely depends on the concentration of photoelectrons. By means of intensified charge coupled device (ICCD) images, Ebert et al. revealed that the active seed electrons ahead of the main streamer head

undergo discrete avalanches toward the main streamer, which first grow into several separate clusters of electrons (which look like spheres) and then become streamer branches [9]. These observations experimentally validate the previous theory of positive streamers proposed by models.

The above studies mainly focus on the macroscopic characteristics of volume positive streamer discharges (i.e., their profile and branching). In addition, the microscopic mechanisms responsible for the formation and evolution of positive streams are relatively well understood. However, the relation between microscopic and macroscopic phenomena is not well understood. The question how the microscopic processes determine the macroscopic behavior (e.g., the streamer velocity, radius, branching, etc) remains open.

The interaction between positive streamers and dielectric (catalyst) materials is extremely important for various plasma applications, e.g. in a packed bed DBD used for plasma catalysis. Kim et al. observed numerous surface positive and negative streamers in packed bed DBD experiments [20–22], depending on the discharge time and voltage, which play an important role in facilitating the interaction between short lived radicals and a catalyst surface. However, positive surface streamers behave quite differently from negative surface streamers. Indeed, positive surface streamers can more easily be induced under the same conditions, and then spread over a larger area [20–22]. In addition, they keep their branching characteristics similar to the dynamics in the gas phase, during propagation along a dielectric (e.g., catalyst pellet) surface [20–22]. These experiments, although very interesting, could only provide qualitative observations. Yan et al. [23] and Babaeva et al. [16] explored the interactions between positive streamers and regular electrodes and dielectrics, respectively, by means of fluid and hybrid models, and the simulations of Babaeva et al. have achieved qualitative agreement with experimental results in [24]. They both point out that an intense sheath (with a strong electric field) can be formed in front of the electrode or dielectric, which corresponds to a so-called 'floating surface discharge' described in this work. However, the shape of the dielectric material in practical plasma applications (such as plasma catalysis) can be very complicated with various dielectric pores, which can effectively increase the surface area of the material exposed to the plasma. Consequently, there is a need for a more detailed understanding of the interaction mechanisms between positive streamers and structured dielectric surfaces. Such insights into microscopic plasma behaviour in small-scale dielectric pores can be obtained by particle-based simulations.

Therefore, in the present study, we investigate the microscopic mechanisms of the formation and propagation of both volume and surface streamers along a dielectric surface, for both positive and negative streamers, by a combination of 2D implicit particle-in-cell/Monte Carlo collision (PIC/MCC) simulations and experiments. We analyze in detail the physical phenomenon of the 'floating surface discharge' in positive streamer propagation. These insights are then used to explain the characteristics of the interaction between positive surface streamers and dielectric surfaces, such as observed in a packed bed DBD used for plasma catalysis. The microscopic interaction mechanisms between a positive streamer and various dielectric pores is also explored.

2. Experimental setup and simulation method

Figure 1 (top) schematically illustrates the experimental setup, which includes a discharge reactor, a nanosecond pulsed power supply, an electrical measurement system and a camera system. The reactor consists of a pin-to-plate electrode configuration, in which the pin electrode is made of stainless steel with a radius of 0.4 mm, and the grounded plate electrode is a stainless steel disc covered by a 1 mm thick ceramic plate (Al_2O_3 ceramic with dielectric constant). The discharge gap can be adjusted between 0-15 mm and is fixed at 4 mm in this experiment. The reactor is driven by a nanosecond pulse power supply (HVP-20, China), which provides a maximum peak voltage of 20 kV, a variable pulse repetition rate of 0-15 kHz, an adjustable rise/fall time of 50-500 ns, and an adjustable pulse peak width of 0-1 ms. A pulsed voltage waveform with a peak voltage of 17 kV, a repetition rate of 1 kHz, a total pulse duration time of 200 ns (trapezoidal shape, including a peak width of 100 ns, a rise time of 50 ns, and a fall time of 50 ns) is applied. The measured voltage and current waveforms (for both positive and negative streamers presented in figure 2) are plotted in figure 1 (bottom). The applied voltage and discharge current are measured by voltage and current probes (Tektronix- P6015A, Pearson Current Monitor-4100), and recorded by an oscilloscope (Tektronix, TDS5054B, 500 MHz). Wavelength averaged 2D space resolved and time resolved images of the discharge are taken by an ICCD camera (Andor iStar DH334T). The gate width of this ICCD camera is 5 ns. The effective spatial resolution of the ICCD camera is 0.02 mm, calculated

using the discharge gap width (4 mm) divided by the vertical length of ICCD images (about 200 pixels). To synchronize the nanosecond pulsed power supply and the ICCD camera, two output signals from the digital delay generator (Stanford Research Systems, model: DG 645) are used to trigger the power supply and the ICCD camera, respectively. To observe both the volume discharge and the surface discharge profiles at the same time, the ICCD camera is aligned so that the angle between the line of sight of the optical observation and the dielectric surface on the grounded electrode is 20°. All experiments are carried out in air at atmospheric pressure.

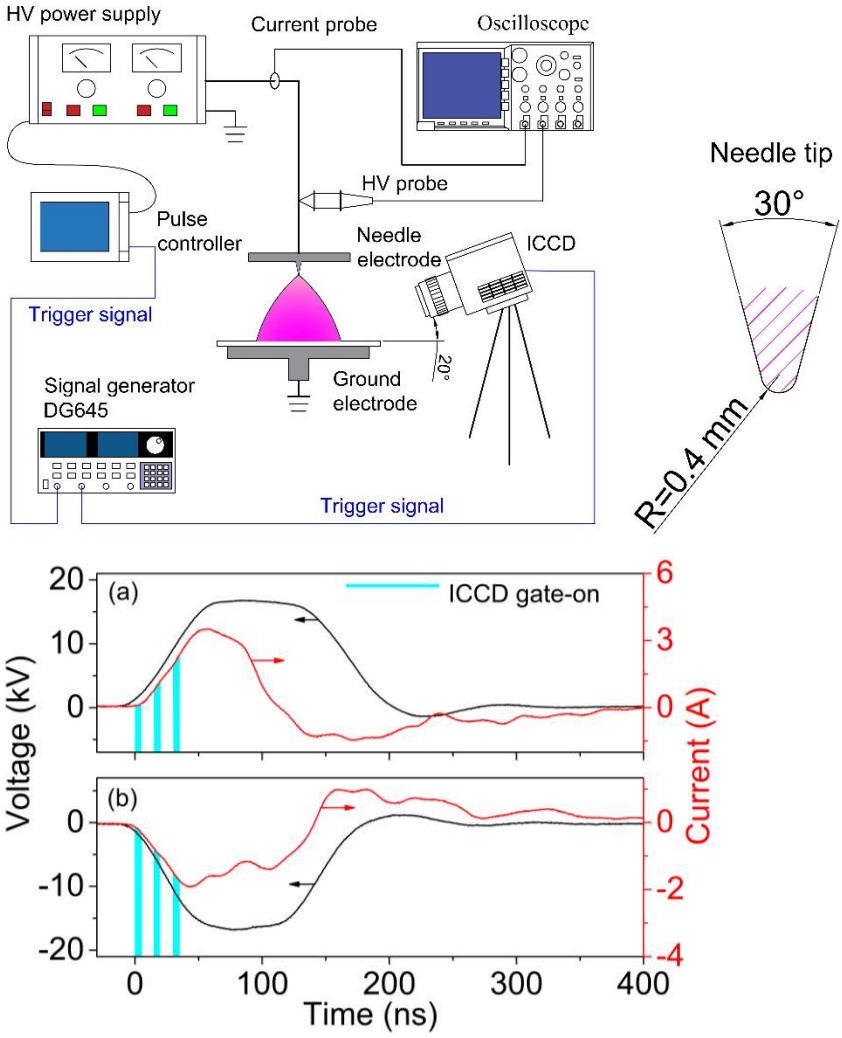

Figure 1. Schematic of the pin-to-plate DBD reactor including the plasma diagnostics used in this work (top), and measured voltage and current waveforms (bottom), for positive (a) and negative (b) streamers. The top part also shows the dimensions of the pin.

A PIC/MCC simulation, described in detail in [25,26], is used to study the plasma streamer evolution in this pin-to-plate DBD. A schematic of the simulation region is shown in figure 2. As the streamer branching behavior is essentially in three dimensions, we first trace the movements of the simulated particles under the effect of the electric field in 3D cartesian coordinates (X, Y, Z), and then convert the particles' coordinates to 2D cylindrical geometry (R, Z) [18,27] (i.e. $X^2 + Y^2 = R^2$) to calculate the plasma density for the field solver (Poisson equation). Later the electric field solved in cylindrical geometry (R, Z) will be converted into cartesian coordinates (X, Y, Z) for particle tracing (both coordinates and velocities). This is typically how the cylindrical PIC model handles the particles and Poisson equation for high numerical accuracy [25,26]. In this way, the simulated particle motion, and the consequent streamer branching are more realistic. However, the mirrored streamers may repel each other, if they are located close to the coordinate center due to the same polarity, causing an asymmetry in the streamer profile. We, thus, place the seed particles with a distance r=2 mm or 4 mm (the mirrored distance is

double) away from the coordinate center, which is much larger than the main streamer bulk (mostly smaller than 0.5 mm), to reduce the interactions between mirrored streamers. As the simulated results are qualitatively consistent with the experimental observations (shown below), including the streamer evolution and branching characteristics, we consider this modeling approach reasonable. To study the interaction of the surface discharge and a pore, the position of the seed electrons is moved to the left in figure 2(b) compared to the setting for non-porous dielectrics shown in figure2(a). The streamer is generated at the position of the seed particles and propagates downwards until it arrives at the opposite electrode and initiates a surfaces discharge that propagates radially along the dielectric. In the scenario illustrated by figure 2(b) the surface discharge needs to propagate some distance radially until it arrives at the pore. In this way the interaction of the surface discharge with the pore can be studied separately from the initial streamer.

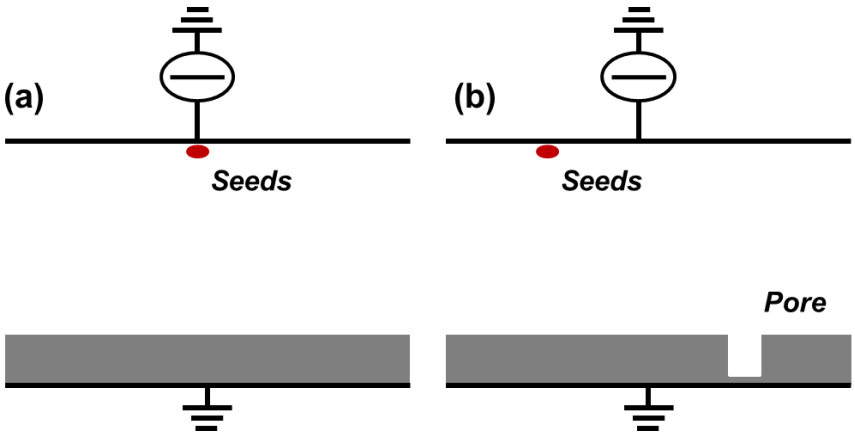

Figure 2. Schematic of simulation region with initial seed particles, for streamer propagation towards a non-porous (a) and porous (b) dielectric.

Due to the short gap distance (4 mm), we only simulate the streamer propagation for a maximum of 3 ns, which is more than enough time for the streamer to reach the bottom electrode and to induce a surface discharge. As the simulation time is much shorter than the rise/fall time of the voltage pulse in the experiments (50 ns), we simulate only the fraction of the pulse, when the voltage is maximum/minimum. Thus, in order to simplify the simulations, we apply a DC voltage of 17 kV/-17 kV (instead of a pulsed voltage) to the top electrode, to trigger the positive/negative streamer, respectively. This does not affect the interaction between the plasma and the dielectric. Dry air at atmospheric pressure and 300 K gas temperature is considered as the discharge gas, with a constant density of background molecules (N_2, O_2). Electrons, O_2^-, O_2^+ and N_2^+ ions are traced in the simulation. To account for the needle electrode in the experiments, which triggers the streamer discharge, 20 seed super-particles of each species (electrons, O_2^-, O_2^+, and N_2^+ ions) are placed right below the top (needle) electrode (around 0.1 mm below), with an initial weight ω_p equal to 10^4. Note that each super-particle represents a number of real particles, as defined by their weight. Hence 1 initial super-particle corresponds to 10^4 real electrons or ions. The weight of the super-particles will automatically increase with the streamer evolution by the particle merging algorithm (explained below). Their initial velocities are sampled from a Maxwellian distribution with an average energy of 2 eV for the electrons and 0.026 eV for the ions. A plasma streamer is observed to propagate from the top towards the bottom electrode based on the seeded super-particles under the effect of the applied voltage. Once the electrons and ions arrive at the dielectric, they will accumulate on the dielectric surface, and contribute to surface charging of the adjacent grids. The particles will be removed from the simulation once they arrive at the electrode or move out of the simulation range.

The simulation geometry is 5×8.3 mm (height×width), and uniformly divided into 1024×1700 cells, with a mesh size around 5 μm. The electron impact collisions taken into account in the model are elastic collisions, excitation, ionization and attachment reactions with N_2 and O_2 gas molecules, as explained in [28] and shown in table 1. The collision cross sections are adopted from the LXCat database [29]. Elastic and charge transfer reactions between ions and gas molecules are also included in the model, and the corresponding cross sections are taken from [30,31]. As these reactions between heavy particles (ions and molecules) are not important for the short

simulation time in this work (in the order of ns) [32], we do not list them here. As the simulation time for streamer evolution is only on the ns scale in this work, and the ions hardly move, we do not consider dissociative detachment of negative ions due to collisions with metastable molecules and Penning ionization.

Table 1: Electron impact reactions included in the model, with the cross sections adopted from the LXCat database [29].

Reaction	Threshold (eV)	Reference
Electron-impact ionization		[29]
$e + O_2 \rightarrow 2e + O_2^+$	12.06	
$e + N_2 \rightarrow 2e + N_2^+$	15.58	
Attachment		[29]
$e + O_2 \rightarrow O_2^-$		
Elastic collision		
$e + O_2 \rightarrow e + O_2$		
$e + N_2 \rightarrow e + N_2$		
Electron-impact excitation		[29]
$e + O_2 \rightarrow e + O_2^*$	0.98	
$e + O_2 \rightarrow e + O_2^*$	1.63	
$e + O_2 \rightarrow e + O_2^*$	6.0	
$e + O_2 \rightarrow e + O_2^*$	8.4	
$e + O_2 \rightarrow e + O_2^*$	10.0	
$e + N_2 \rightarrow e + N_2^*$	6.169	
$e + N_2 \rightarrow e + N_2^*$	7.353	
$e + N_2 \rightarrow e + N_2^*$	7.362	
$e + N_2 \rightarrow e + N_2^*$	8.165	
$e + N_2 \rightarrow e + N_2^*$	8.399	
$e + N_2 \rightarrow e + N_2^*$	8.549	
$e + N_2 \rightarrow e + N_2^*$	8.89	
$e + N_2 \rightarrow e + N_2^*$	9.7537	
$e + N_2 \rightarrow e + N_2^*$	11.032	
$e + N_2 \rightarrow e + N_2^*$	12.771	
$e + N_2 \rightarrow e + N_2^*$	13.37	
$e + N_2 \rightarrow e + N_2^*$	13.382	
$e + N_2 \rightarrow e + N_2^*$	14.0	

Table 2: Summarized conditions for both experiment and simulation.

Conditions	Experiment	Simulation
Gap distance	4 mm gap + 1mm dielectric	4 mm gap + 1mm dielectric
Working gases	Atmospheric pressure air	Atmospheric pressure air
Applied voltage	Pulse source with peak voltage of ±17 kV, repetition rate of 1 kHz	DC voltage: ±17 kV

Gate width of ICCD camera	5 ns	
Boundary conditions	Open	Left: axisymmetric Right: Neumann (Partial derivative of the electric potential is fixed)
Algorithm		Poisson equation: Multi-grid Transport equations: Newtonian motion equations in leap-frog scheme Merging algorithm: 'three-two' particle merging
Photo-ionization	O_2 is ionized by absorbing photons emitted by N_2^*	Zheleznyak's photo-ionization model

Since the number of simulated particles will rapidly increase due to the ionization avalanches after a certain time, a 'three-two' particle merging algorithm [33] is applied to restrict the number of particles: when the number of each type of super-particle exceeds 50 in each grid, three particles are combined into two particles ensuring both conservation of momentum and energy. We employ the widely used stochastic version of Zheleznyak's photo-ionization model [10,18,19,34,35] to account for photo-ionization, i.e. ionization of O_2 molecules after absorbing photons emitted by excited N_2 molecules, with a wavelength between 98 and 102.5 nm. This photo-ionization model was originally built based on experimental measurements, and directly calculates the number and location of photo-ionization events. The experimental measurements provide a photo-ionization coefficient, which indicates how many ionizing photons are produced corresponding to each electron-impact ionization. The number of photo-ionization events is then calculated when an electron-impact ionization happens based on the local electric field together with a quenching factor. The absorption length of a UV-photon is calculated based on its wavelength (between 98 to 102.5 mm) with a random isotropic direction. More details can be found in ref. [19]. The initial weight of newly generated particles by photo-ionization is always equal to 1. A fixed secondary electron emission coefficient of 0.1 on the bottom dielectric is set for both electrons and the three different types of ions [32]. As we do not trace the movement of photons in this photo-ionization model, photon-induced secondary electron emission is ignored, similar to [10,18,19,34,35]. The final number of super-particles is around five million. The Poisson equation is solved based on a multi-grid algorithm, and the movement of super-particles is realized based on Newtonian motion equations in leap-frog scheme. When solving the Poisson equation, an axisymmetric boundary condition is set for the left side of the simulation range, while the right side is set as Neumann (partial derivative of the electric potential is fixed at 0) boundary. The conditions for experiment and simulation are summarized in table 2 for easy comparison. Our PIC/MCC model is a parallel code based on MPI. It takes 1-2 days for each simulation by 4 or 5 cores, and consumes around 20GB memory on our server, which has 44 cores (3.7 GHz) and 256GB.

3. Results

3.1 Experimental observations of the propagation of positive and negative streamers above planar dielectric surfaces

Figure 3 shows temporal sequences of 2D space resolved and wavelength averaged images taken by a fast ICCD camera under the conditions outlined in section 2. The temporal sequences, at which observations are taken, are indicated in figure 1 (bottom) (a) for a maximum applied voltage of +17 kV, and (b) for a minimum applied voltage of -17 kV. Correspondingly, the top panel of figure 3 shows the propagation of a positive streamer, while the propagation of a negative streamer is shown in the bottom panel of figure 3. Both streamers are initially generated at the needle electrode and develop toward the bottom dielectric (placed on top of the bottom electrode).

Due to the small gap and limited resolution in the experiments, only two spatial branches in the positive streamer and one single negative streamer are observed in figure 3(c) and figure 3(f), respectively. However, remarkably, many branches appear along the dielectric when the positive streamer approaches and arrives at the dielectric (figure 3 (c)), whereas the negative surface streamer develops uniformly on the dielectric surface towards all directions without any branches. This behaviour is consistent with experimental observations for the propagation of positive and negative surface streamers on pellets in a packed bed DBD [21,22].

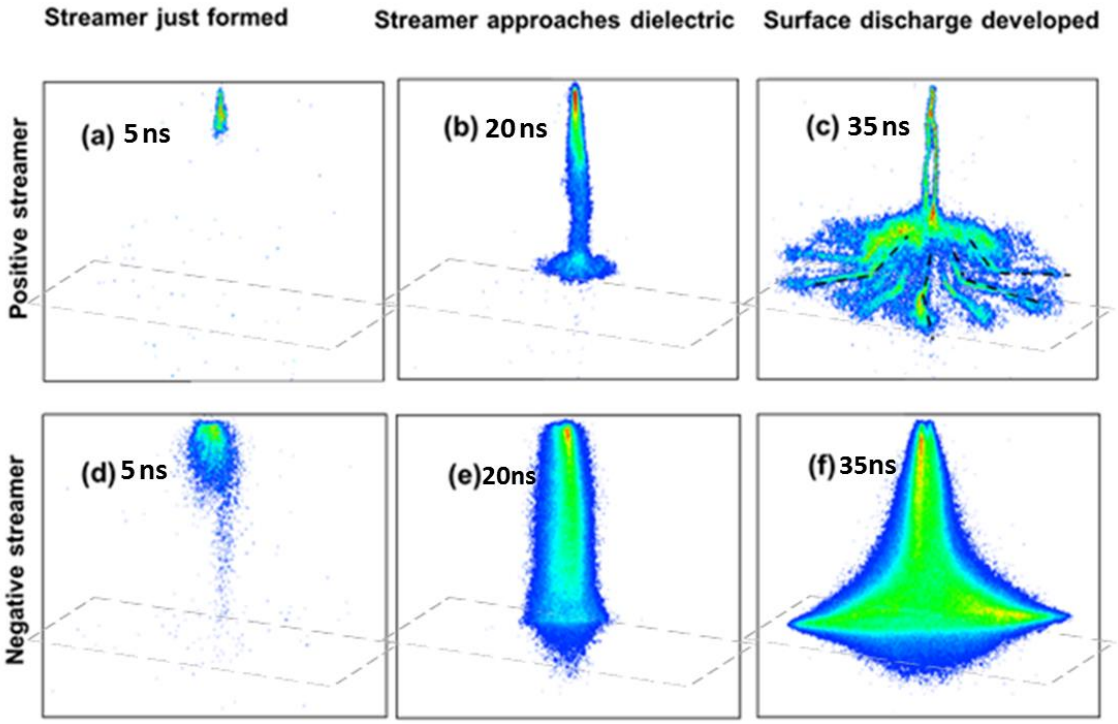

Figure 3. 2D space and time resolved light intensity evolutions (a.u.) measured by a fast ICCD camera: (a, b, c) positive streamer, (d, e, f) negative streamer. The top (needle) electrode is located at the top and at the center of the horizontal axis, while the bottom electrode is schematically indicated, for the sake of clarity. The black dashed lines in (c) are added to illustrate that the branches of the positive surface streamer are bent. A trapezoidal pulsed voltage waveform with a peak voltage of 17 kV is applied (see figure 1). The light intensities for positive and negative streamers are normalized to different values.

Furthermore, it is worth to note that almost all branches of the positive surface streamer are bent, as indicated by the black dashed lines in figure 3(c). This suggests that the gas phase primary streamer does not reach the dielectric, which agrees qualitatively with our PIC/MCC simulation results discussed below, and agrees well with the observation in [16,23] based on fluid models. The gas phase primary streamer also splits into many branches caused by photo-ionization [13] above the dielectric, after which the streamer branches develop separately in the horizontal direction and propagate along the dielectric surface, inducing positive surface streamer discharges in different directions. Thus, the many branches of the surface discharge actually originate from the gas phase primary streamer branches.

Due to the limited spatial resolution of the ICCD camera we cannot observe the dark electrode/dielectric and we cannot measure the width of the small gap between the gas phase primary streamer and the bottom dielectric. We will explore this behaviour in detail based on our PIC/MCC simulation results shown in figure 4, which illustrates an interesting physical phenomenon of a floating surface discharge. In addition, we will demonstrate that the underlying mechanisms for positive and negative surface streamers are completely different.

3.2 PIC/MCC simulation results for the propagation of positive and negative streamers above planar dielectric surfaces

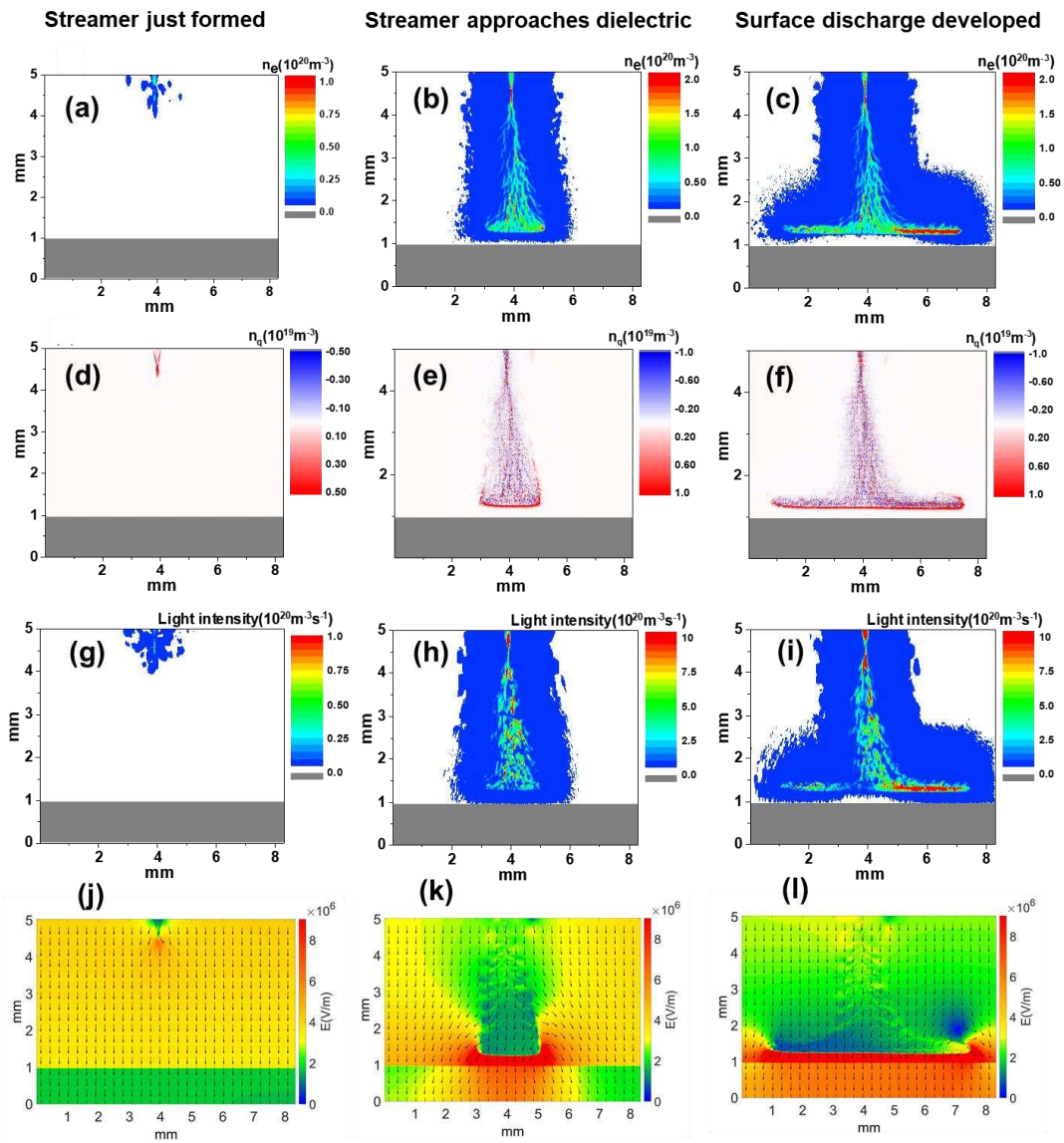

Figure 4. (a,b,c) Electron density, (d,e,f) charge density, (g,h,i) light intensity, and (j,k,l) electric field evolution (the absolute value of the electric field is plotted and the arrows indicate the directions), during positive streamer propagation, calculated based on the PIC/MCC simulation, when 17 kV is applied at the top electrode. The dielectric covering the bottom electrode is indicated in grey (a-i).

Figure 4 presents the space and time evolution of the electron density, charge density, light intensity (obtained from the calculated total electron impact excitation rate by counting the number of excitation collisions which the electron experiences at each grid per second) and electric field resulting from the PIC/MCC simulation, when 17 kV is applied to the top electrode. Note that no time-scale is indicated in the simulation results, because in our simulations we only assumed seed electrons at the 'tip' location to observe the streamer evolutions, while in reality there are abundant background electrons, affecting the streamer speed. The timing in the simulation is thus not very realistic, but the qualitative time-evolution and mechanism of streamer propagation, as well as the streamer profiles revealed from the simulation, stay valid and meaningful.

When the streamer is just formed, we clearly observe a positive space charge region in front of the streamer head (red layer). This positive space charge region is caused by the acceleration of electrons towards the pin electrode, which serves as anode. This movement of electrons leaves behind a positive space charge at the streamer head, which generates a strong electric field around the streamer head (as shown in figure 4(j)). The electrons nearby further induce abundant electron-impact ionizations under the effect of this strong electric field. Simultaneously, the number and location of photo-ionization events per electron-impact ionization are calculated

according to the photo-ionization model based on the local electric field. These photoelectrons are accelerated towards the anode by the electric field and, thus, electron avalanches caused by photoelectrons near the streamer head are generated, as indicated by the many small dots in figure 4(a) and (g), corresponding to the spheres observed in experiments [9]. Most of these avalanches overlap and become part of the propagating streamer, which facilitates the streamer propagation and branching. The positive space charge region (red layer) broadens as a function of time (as revealed from figure 4 (d,e,f)), and keeps inducing strong electric field (shown in figure 4 (j,k,i)) and consequent avalanches of photoelectrons over a larger area.

However, two conditions need to be satisfied for the generation of avalanches: (i) enough free electrons must be present close to the streamer head and (ii) these free photoelectrons must be able to propagate a sufficient distance within the high electric field close to the streamer head in order to be multiplied by collisions and cause the avalanche. When the streamer approaches the dielectric (see figure 4(b,e,h,k)), the distance between the streamer head and the dielectric surface becomes too small, so that the number of photoelectrons generated in front of the streamer head significantly decreases. Thus, also the formation of electron avalanches is attenuated. As the streamer propagation results from the avalanches in front of the streamer head, the propagating streamer stops moving in the forward direction, and when it reaches the dielectric, it develops horizontally under the influence of the electric field (see figure 4(k,l)) caused by the positive space charge region around the streamer head, as shown in figure 4(c,f,i), i.e. a floating positive surface discharge develops above the dielectric surface. This is in qualitative agreement with the experimental observations in figure 3(c), and with the results in [23] based on a fluid model with a similar pin-to-plate discharge configuration. This is probably one of the reasons for the experimentally observed abundant branches of the positive surface discharge in figure 3(c).

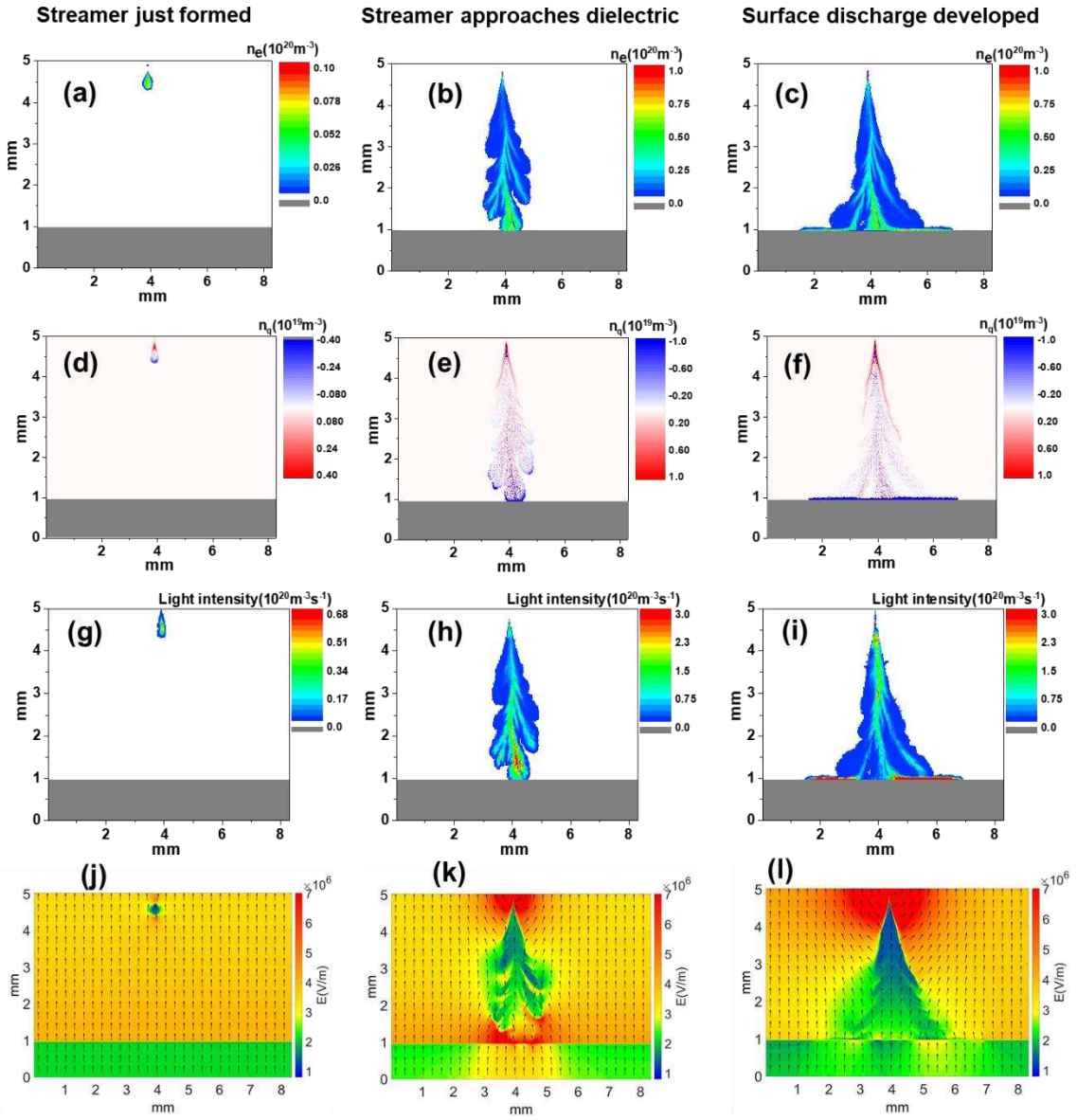

Figure 5. (a,b,c) Electron density, (d,e,f) space charge density, (g,h,i) light intensity and (j,k,l) electric field evolution (the absolute value of the electric field is plotted and the arrows indicate the directions), during negative streamer propagation, calculated based on the PIC/MCC simulation, when -17 kV is applied at the top electrode. The dielectric covering the bottom electrode is indicated in grey (a-i).

For comparison, we plot the time evolution of the electron density, space charge density and light intensity (obtained from the electron impact excitation rate at each grid per second) during negative streamer propagation in figure 5. The results are obtained from the PIC/MCC simulation, when -17 kV is applied to the top electrode. For negative streamer propagation, photo-ionization is known to be negligible [28,36,37], since it induces an ionization rate which is two orders of magnitude smaller than the electron impact ionization rate. Thus, we did not include photo-ionization in the simulations that yield the results shown in figure 5 in order to observe the streamer paths clearly. After some initial avalanches caused by the presence of seed electrons, a negative streamer gradually develops, as shown in figure 5(a). However, in contrast to the positive streamer case, electrons are now pushed away from the pin electrode, which serves as cathode (as revealed by the arrows of electric field in figure 5(j)). Consequently, a negative space charge region (blue layer) is formed around the streamer head, which generates a strong electric field and accelerates electrons close to the streamer head to move towards the anode, yielding streamer propagation (see figure 5(d), (g) and (j)). As the propagation of the negative streamer does not rely on the electron sources (photoelectrons) in front of the streamer head, the negative streamer will finally arrive at the

dielectric, and the electrons will charge the dielectric surface negatively, contributing to a non-uniform surface charge distribution (blue layer in figure 5 (f), with more charging at the main streamer location and less charging at the streamer edge, generating a horizontal electric field along the dielectric surface). The accumulated electrons on the dielectric surface will induce an extra electric field along the surface, and induce a surface discharge on the dielectric (as seen in figure 5 (c,f,i,l)). Although there are also branches in the gas phase negative streamer, their number is much lower than in the positive streamer case, which can be revealed by comparing figure 4 (a,b,c) and figure 5 (a,b,c).

3.3 Interactions between positive/negative streamers and dielectric (catalyst) pore

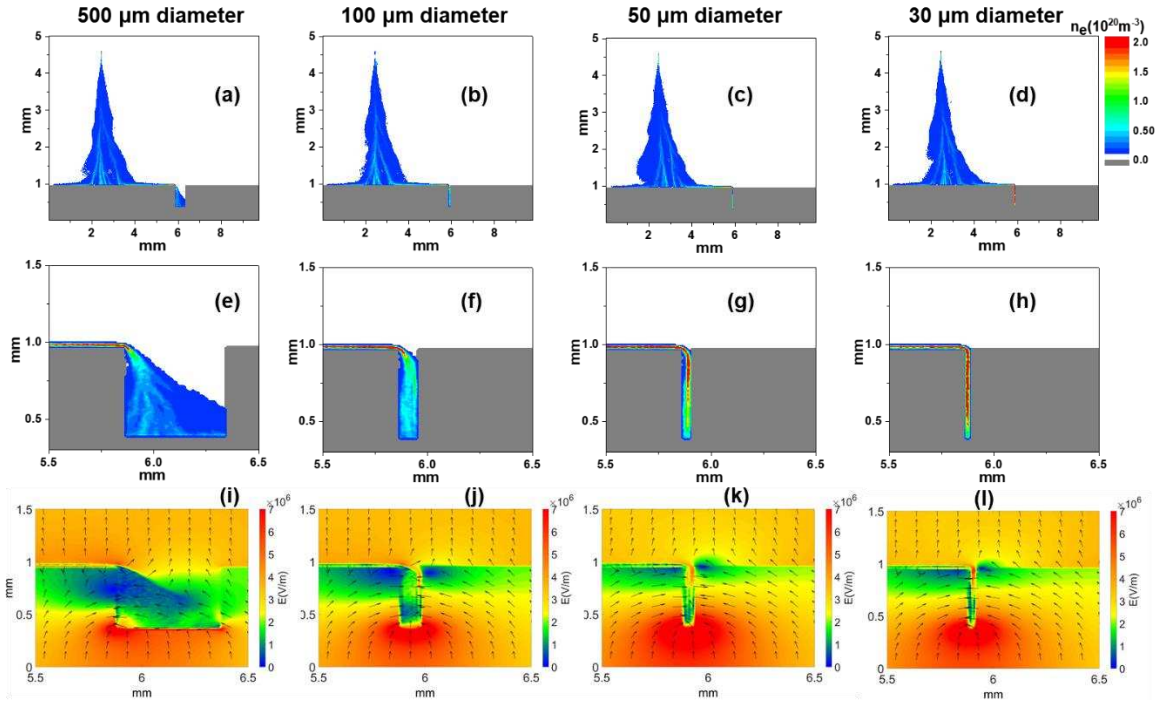

Figure 6. Electron density distribution, illustrating the evolution of a negative plasma streamer inside the discharge (a,b,c,d), and near the catalyst pore in the bottom dielectric (e,f,g,h), as well as the electric field distribution (the absolute value of the electric field is plotted and the arrows indicate the directions) near the catalyst pore in the bottom dielectric (i,j,k,l) with a pore diameter of (a,e,i) 500 μm, (b,f,j) 100 μm, (c,g,k) 50 μm, and (d,h,l) 30 μm. The top pin electrode is driven by -17 kV.

The interaction of plasma streamers with surfaces made of different materials and structures is of outmost importance for a variety of applications such as plasma catalysis. A detailed understanding of this plasma-surface interaction is essential for knowledge-based optimization of these plasma processes. The phenomenon of floating positive surface discharges as a consequence of positive streamers approaching dielectric surfaces (shown in figure 3) was also observed in [16,23], based on fluid models. In these works, the authors studied the effect of secondary electron emission and the choice of the dielectric surface material on the floating surface discharge and found that the secondary electron emission decreases the 'floating' gap (between the plasma and the dielectric), whereas the flux of ions to the surface increases as a function of the relative permittivity of the dielectric [23]. Often such surfaces are structured, i.e. they contain catalyst (dielectric) pores, which determine the effective catalyst surface area exposed to the plasma species. The effects of these pores on the interaction of streamers with boundary surfaces are not well understood. Therefore, in this section, we focus on such interactions between the plasma and catalyst (dielectric) pores with different sizes (i.e., diameters and depths).

Figures 6 and 7 show the plasma density distributions near and inside a catalyst (dielectric) pore with different diameters, when a negative and a positive streamer reaches the pore, respectively. As indicated in figure 6, the negative streamer starts developing on the dielectric surface after reaching the bottom dielectric. Since the pore diameters studied here (i.e., 30-500 μm) are all larger than the Debye length (ca. 2 μm) in the streamer head, the

plasma streamer can further penetrate into the catalyst pores. Indeed, we demonstrated in [38] that the Debye length is an important criterion for negative streamer penetration into catalyst pores. The electrons charge the pore sidewall non-uniformly and, thus, induce an extra electric field along the pore surface, which results in a discharge enhancement. The electric field becomes more pronounced at smaller pore diameter, as revealed at the right side of the pore entrances in figure 6 (i,j,k,l). This induces an enhanced discharge in figure 6 (e,f,g,h), and is consistent with the observations in [38,39], i.e., the plasma density reaches a maximum when the pore diameter is close to the Debye length. Calculation results for smaller pore diameter can be found in [38], and the smallest pore diameter could be around 700 nm with enhanced density inside the pore.

However, as indicated in figure 7, the interaction between a positive streamer and a dielectric pore is completely different from the behavior of a negative streamer. Instead of a surface discharge on the dielectric, which is present in case of a negative streamer reaching the surface (see figure 6), a floating surface discharge (with a small gap between the plasma and dielectric) is induced above the surface, when a positive streamer approaches the dielectric. If the pore diameter is large (i.e., larger than the streamer width), the streamer will turn direction and propagate into the pore under the effect of the electric field in the vertical direction, as shown in figure 7 (a,e,i), until the volume and depth in front of it become too small, so that not enough photoionization and avalanches can be produced for sustaining the streamer (around 300 μm from the pore bottom). However, if the pore diameter decreases to 100 and 50 μm, the streamer propagates into the pore and additionally a surface streamer branches above the pore, since the photoionization inside the pore provides enough seed electrons and, thus, induces this additional streamer branch, which is clearly revealed in figure 7 (f) and (g). The discharges can actually reach the vertical pore sidewall, inducing an enhanced electric field (see figure 7 (f,g)) and consequently a higher density, which may produce more photoionization and avalanches in a smaller volume, and allow the streamer to penetrate a bit deeper. This implies that there are two different interaction mechanisms by which positive streamers can interact with dielectric surfaces, and depending on the dominant mechanism, positive streamers can reach the dielectric surfaces or not.

The latter is defined by the relative direction between the applied electric field and the dielectric surface. Outside the pore, the electric field is perpendicular to the dielectric surface (as indicated by the electric field line in figure 4(j)), and the electrons can only be pushed away from the dielectric (as the electrons move against the direction of the electric field). The electrons next to the main streamer above the dielectric are attracted toward the streamer head under the effect of the electric field at the streamer head (see figure 4 (k,l)), sustaining the floating surface discharge. However, inside the pore, the electric field generated by the positive space charge inside the streamer head is not perpendicular to the dielectric surface (pore sidewall). Thus, electrons that propagate in the streamer channel can reach the dielectric. The surface discharge can thus happen along the pore sidewall. Furthermore, as the electrons are accelerated parallel to the pore sidewall, the number of photoelectrons and the travelled distance for their avalanche are not affected by the distance between the streamer and the dielectric walls. Thus, the positive streamer can propagate into the pore and along the sidewall. Therefore, we conclude that the angle between the direction of the electric field and the surface of the dielectric wall material determines whether there will be a floating surface discharge (the height of the floating surface discharge above the material is the largest at an angle of 90°) or a discharge that propagates along the surface at zero height (at an angle of 0°).

These mechanisms are very important for a better understanding of the interactions between positive streamers and dielectric material in various applications, especially in packed bed DBDs used for plasma catalysis. Indeed, the shapes of the dielectric pellets (typically coated with catalysts) can be very complicated, due to the inherent macro- (~10 μm) or meso-pores (~10 nm). As a result, the relative direction between the electric field and the dielectric surface changes all the time during the streamer evolution, which probably induces complicated interactions between plasma streamers and dielectric materials.

If the pore diameter decreases further to 30 μm (see figure 6 (h)), the pore seems to be too narrow to provide sufficient photo-ionization and electron avalanches, and the streamer cannot propagate into the pore anymore.

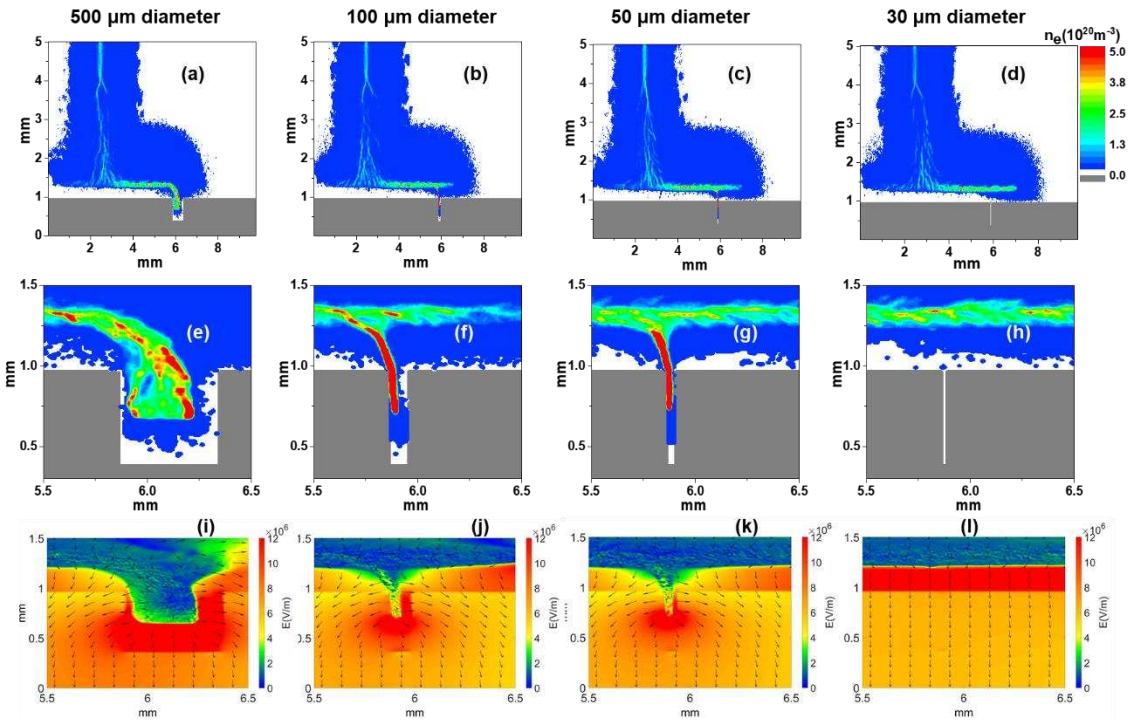

Figure 7. Electron density distribution, illustrating the evolution of a positive plasma streamer inside the discharge (a,b,c,d), and near the catalyst pore in the bottom dielectric (e,f,g,h), as well as the electric field distribution (the absolute value of the electric field is plotted and the arrows indicate the directions) near the catalyst pore in the bottom dielectric (i,j,k,l) with a pore diameter of (a,e,i) 500 µm, (b,f,j) 100 µm, (c,g,k) 50 µm, (d,h,l) 30 µm. The top pin electrode is driven by 17 kV.

To obtain further insight, we also study the influence of the pore depth on the positive streamer propagation, when the floating surface streamer propagates over the pore. As shown in figure 8 (a), the streamer can easily branch into the pore, for a pore depth of 600 µm and a pore diameter of 50 µm. The discharge inside the pore is enhanced in this case, i.e. the electron density is maximum inside the pore. If the pore depth is reduced to 400 µm (figure 8 (b)), there is still an enhanced but shorter streamer branch, ending at the pore orifice, even when the electric field is enhanced at the pore entrance (see figure 8 (f)), which denotes that significant photo-ionization and electron avalanches happen inside the pore, but the streamer branch forms just outside of the pore, i.e. 400 µm seems to be the minimum pore depth for streamer formation inside the pore under these discharge conditions. When the pore depth is further reduced to 300 µm (figure 8 (c)), a very short branch appears above the pore with a bit curved electric filed distribution (figure 8 (g)), but at 150 µm pore depth, it is not observed anymore (see figure 8 (d)).

Therefore, we conclude that the Debye length is not the criterion for positive streamer penetration into pores, in contrast to the situation for negative streamers. Indeed, both the pore diameter and depth affect the evolution of a positive streamer inside the pores. Especially for a plasma density of the order of 5×10^{20} m^{-3} (such as observed in this work), a 30 µm pore diameter and 400 µm pore depth are the minimum pore dimensions for positive streamer penetration inside a pore. Smaller pore dimensions do not provide enough room for photo-ionization in front of the positive streamer head, which is required to provide seed electrons for the propagation of such streamers. Such electrons in front of the streamer head are necessary for positive streamer propagation into the pore. In other words, large catalyst pores can always induce plasma streamer branches, when the positive streamer approaches, even without the need of contact with the catalyst surface.

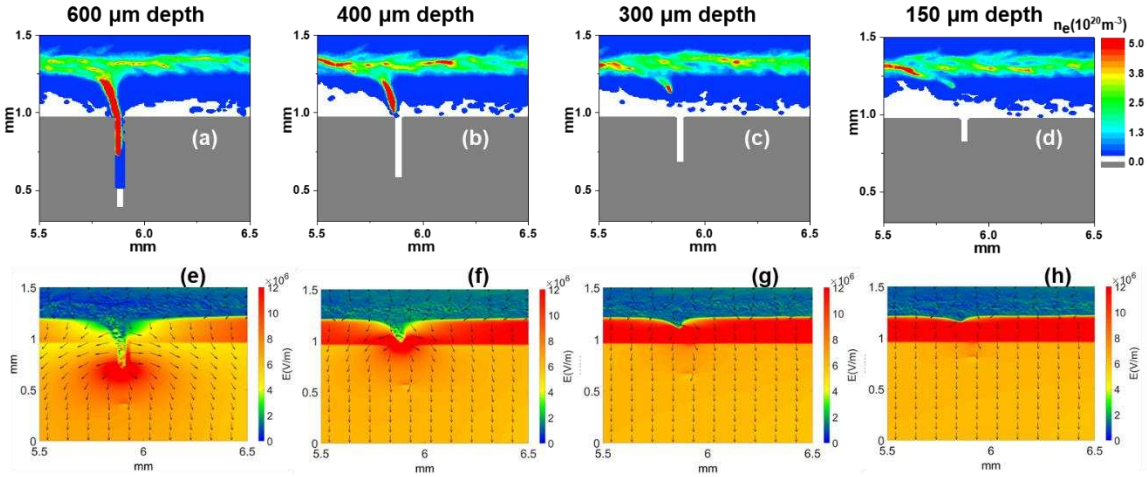

Figure 8. Electron density (a,b,c,d) and electric field (e,f,g,h) distribution (the absolute value of the electric field is plotted and the arrows indicate the directions), near and inside a catalyst pore inside the bottom dielectric, with a pore depth of (a,e) 600 μm, (b,f) 400 μm, (c,g) 300 μm, (d,h) 150 μm, and a pore diameter of 50 μm. The top pin electrode is driven by 17 kV.

4. Conclusions

In conclusion, based on ICCD camera observations and PIC/MCC simulations we demonstrated that positive and negative streamers behave quite differently in volume DBDs. There is always a positive or negative space charge region in the positive or negative streamer head, respectively, which promotes the streamer propagation. However, the positive streamer propagation always requires a source of electrons (mainly provided by photoelectrons) in front of the streamer head. Therefore, when the positive streamer approaches a dielectric surface, the distance between the streamer head and the dielectric surface becomes too small to maintain enough photo-ionization and the streamer cannot propagate forward anymore, but it develops horizontally above the dielectric, inducing a floating surface discharge. The characteristics of this floating surface discharge, i.e. its direction of propagation and its height above the surface, strongly depend on the relative orientation between the electric field and the dielectric surface. The distance from the dielectric surface at which the streamer propagates is found to be reduced to zero, if the electric field generated by the space charge located inside the streamer head is parallel to the dielectric surface, e.g. along the sidewall of catalyst pores. The streamer propagation mechanism for negative streamers is completely different, and they can arrive at the dielectric surface, inducing a negative surface discharge on the dielectric.

Both, gas phase volume and surface positive streamer discharges, are induced by a space charge region (red layer in figure 4(d), (e), (f)) around the streamer head, while in negative streamers only the gas phase propagation depends on the charge region (blue layer in figure 5(d), (e)), whereas the surface propagation is dominated by the non-uniform surface charge distribution (blue layer in figure 5(f)).

Unlike the interaction mechanism between a negative streamer and dielectric pores, the Debye length seems not to be the criterion for positive streamer penetration into dielectric pores, but both the pore diameter and depth affect the evolution of a positive streamer into the pores. Hence, large dielectric pores can always induce plasma streamer branches, when the positive streamer approaches a pore under the effect of photo-ionization, if the pore is large enough to provide sufficient photo-ionization as the basis for the streamer propagation into the pore.

The present study provides a better understanding of positive and negative streamer discharges. We report for the first time the interactions between a positive streamer and dielectric pores, which is important for practical applications, e.g., in plasma catalysis, as it determines the plasma spreading along the dielectric surface. Both the enhanced density and enlarged spreading area could promote the catalysis efficiency, as a high density produces more reactive radicals and the spreading area of the streamer defines the catalyst surface area exposed to the plasma species.

Acknowledgments

We acknowledge financial support from the TOP-BOF project of the University of Antwerp. This work was carried out in part using the Turing HPC infrastructure at the CalcUA core facility of the Universiteit Antwerpen, a division of the Flemish Supercomputer Center VSC, funded by the Hercules Foundation, the Flemish Government (department EWI) and the University of Antwerp. Funding by the German Research Foundation (DFG) in the frame of the Collaborative Research Center SFB 1316, project A5, National Natural Science Foundation of China (No. 12020101005) and the Scientific Research Foundation from Dalian University of Technology (DUT19RC(3)045) is also acknowledged.

References

[1] H.-H. Kim, A. Ogata, and S. Futamura, Appl. Catal. B Environ. **79**, 356 (2008).

[2] J. Van Durme, J. Dewulf, C. Leys, and H. Van Langenhove, Appl. Catal. B Environ. **78**, 324 (2008).

[3] H. L. Chen, H. M. Lee, S. H. Chen, Y. Chao, and M. B. Chang, Appl. Catal. B Environ. **85**, 1 (2008).

[4] J. C. Whitehead, J. Phys. D. Appl. Phys. **49**, 243001 (2016).

[5] E. C. Neyts, K. (Ken) Ostrikov, M. K. Sunkara, and A. Bogaerts, Chem. Rev. **115**, 13408 (2015).

[6] R. Snoeckx and A. Bogaerts, Chem. Soc. Rev. **46**, 5805 (2017).

[7] A. Bogaerts and E. C. Neyts, ACS Energy Lett. **3**, 1013 (2018).

[8] S. Nijdam, F. M. J. H. van de Wetering, R. Blanc, E. M. van Veldhuizen, and U. Ebert, J. Phys. D. Appl. Phys. **43**, 145204 (2010).

[9] U. Ebert, C. Montijn, T. M. P. Briels, W. Hundsdorfer, B. Meulenbroek, A. Rocco, and E. M. Van Veldhuizen, Plasma Sources Sci. Technol. **15**, (2006).

[10] L. Ningyu and P. P. Victor, J. Geophys. Res. Sp. Phys. **109**, A 04301 (2004).

[11] E. M. van Veldhuizen and W. R. Rutgers, J. Phys. D. Appl. Phys. **35**, 2169 (2002).

[12] S. Nijdam, E. Takahashi, A. H. Markosyan, and U. Ebert, Plasma Sources Sci. Technol. **23**, 25008 (2014).

[13] R. Ono and T. Oda, J. Phys. D. Appl. Phys. **36**, 1952 (2003).

[14] Z. Xiong and M. J. Kushner, Plasma Sources Sci. Technol. **23**, 65041 (2014).

[15] B. Bagheri, J. Teunissen, U. Ebert, M. M. Becker, S. Chen, O. Ducasse, O. Eichwald, D. Loffhagen, A. Luque, D. Mihailova, J. M. Plewa, J. van Dijk, and M. Yousfi, Plasma Sources Sci. Technol. **27**, 95002 (2018).

[16] N. Y. Babaeva, D. V Tereshonok, and G. V Naidis, Plasma Sources Sci. Technol. **25**, 44008 (2016).

[17] M. Jiang, Y. Li, H. Wang, and C. Liu, Phys. Plasmas **24**, 102112 (2017).

[18] O. Chanrion and T. Neubert, J. Comput. Phys. **227**, 7222 (2008).

[19] J. Teunissen and U. Ebert, Plasma Sources Sci. Technol. **25**, 44005 (2016).

[20] W. S. Kang, H.-H. Kim, Y. Teramoto, A. Ogata, J. Y. Lee, D.-W. Kim, M. Hur, and Y.-H. Song, Plasma Sources Sci. Technol. **27**, 15018 (2018).

[21] H.-H. Kim, Y. Teramoto, A. Ogata, W. S. Kang, M. Hur, and Y.-H. Song, J. Phys. D. Appl. Phys. **51**, 244006 (2018).

[22] H.-H. Kim, Y. Teramoto, and A. Ogata, J. Phys. D. Appl. Phys. **49**, 415204 (2016).

[23] W. Yan, F. Liu, C. Sang, and D. Wang, Phys. Plasmas **21**, 13504 (2014).

[24] S. A. Stepanyan, A. Y. Starikovskiy, N. A. Popov, and S. M. Starikovskaia, Plasma Sources Sci. Technol. **23**, 45003 (2014).

[25] W. Jiang, H. Wang, Z. Bi, and Y. Wang, Plasma Sources Sci. Technol. **20**, 35013 (2011).

[26] H. Wang, W. Jiang, and Y. Wang, Plasma Sources Sci. Technol. **19**, 45023 (2010).

[27] A. Luque and U. Ebert, J. Comput. Phys. **231**, 904 (2012).

[28] Y. Zhang, H. Wang, Y. Zhang, and A. Bogaerts, Plasma Sources Sci. Technol. **26**, 54002 (2017).

[29] Biagi-v8.9 Database, Www.Lxcat.Net.Lxcat.Net (2015).

[30] V. Vahedi and M. Surendra, Comput. Phys. Commun. **87**, 179 (1995).

[31] A. V Phelps, J. Phys. Chem. Ref. Data **20**, 557 (1991).

[32] Y. Zhang, H. Wang, W. Jiang, and A. Bogaerts, New J. Phys. **17**, 83056 (2015).

[33] G. Lapenta, J. Comput. Phys. **181**, 317 (2002).

[34] M. B. Zheleznyak, A. K. Mnatsakanian and S. V. Sizykh, High Temp., 20, 357-362 (1982).

[35] Y. Li, R. Wang, Q. Zhang, Y. Zhou, H. Wang, and C. Liu, IEEE Trans. Plasma Sci. **39**, 2226 (2011).

[36] N. Y. Babaeva and M. J. Kushner, Plasma Sources Sci. Technol. **18**, (2009).

[37] N. Y. Babaeva and M. J. Kushner, Plasma Sources Sci. Technol. **23**, (2014).

[38] Q.-Z. Zhang and A. Bogaerts, Plasma Sources Sci. Technol. **27**, 35009 (2018).

[39] Q.-Z. Zhang, W.-Z. Wang, and A. Bogaerts, Plasma Sources Sci. Technol. **27**, 65009 (2018).